Modeling groundwater upwelling as a control on river ice thickness

Chas Jones, Knut Kielland and Larry Hinzman

ABSTRACT

The Tanana River flows through interior Alaska, a region characterized by discontinuous permafrost. Studies link degrading permafrost to increased winter river discharge due to greater groundwater (GW) recharge increasing GW input to river baseflow. In winter, interior Alaskan rivers are exclusively fed by GW, which provides an external source of heat. In fact, some portions of rivers fed by GW maintain thin ice cover throughout the winter, or remain ice-free, despite very cold air temperatures. These ice conditions represent a significant danger to rural Alaskans who extensively use rivers for wintertime travel in this largely roadless area. A physically based, numeric model was developed to examine the consequences of permafrost degradation in explaining unfrozen river conditions in the winter. Results show that the ice melt was amplified by increased water column temperatures, flow velocities, air temperature, and snowfall. Abrupt changes in snowfall were illustrated to contribute to decreased ice thickness and more hazardous conditions for winter travelers. The model examines the physical mechanisms that underlie dangerous ice conditions in winter and early spring, and suggests that GW flow parameters need to be better characterized to model mid-winter ice degradation in sub-arctic environments.

Key words | groundwater, heat transfer, ice, model, permafrost, surface water

Chas Jones (corresponding author)
Larry Hinzman
International Arctic Research Center,
University of Alaska Fairbanks,
PO Box 757340,
Fairbanks,
Alaska 99775,
USA
E-mail: *chas@chasjones.com*

Knut Kielland
Institute of Arctic Biology,
University of Alaska Fairbanks,
Fairbanks,
Alaska 99775,
USA

INTRODUCTION

Historically, many Alaskan villages and towns were established along waterways, which served as transportation corridors throughout most of the year. Owing to the limited road network, frozen river systems are still important transportation networks in rural Alaska. Collaborative partnerships were established with several local (non-academic) Alaskans who have extensive experience traveling on Alaskan rivers in all seasons. Their observations on the Tanana River (Jones *et al.* 2013; Schneider *et al.* 2013a, b) mirror those found by Herman-Mercer *et al.* (2011) who reported that rural Alaskans have observed that thin ice was becoming more common on the Yukon River in recent winters. Such ice thinning represents a significant danger to winter travelers.

One potential mechanism for thinning ice relates to changes in permafrost distribution. Ice-rich permafrost is an effective barrier to water transport and recharge (Burt & Williams 1976: Horiguchi & Miller 1980; Kane & Stein 1983), but warming temperatures have caused significant permafrost degradation across the Arctic (Jorgenson *et al.* 2001; Hinzman *et al.* 2005; Romanovsky *et al.* 2010). Permafrost degradation in discontinuous permafrost regions has been described as a potential mechanism for increased hydrologic connectivity between surface and ground water systems. The impermeability of permafrost to water infiltration prevents groundwater (GW) recharge and forces near-surface water to flow laterally and quickly into streams. With permafrost thawing, there is more infiltration to sub-permafrost GW, which delays the rapid runoff from a watershed and allows for more sustained subsurface discharge throughout the winter. Permafrost degradation has been associated with: lake drainage (Yoshikawa & Hinzman 2003); increased daily summer and winter minimum river flows (Smith *et al.* 2007); and increases in winter river

doi: 10.2166/nh.2015.026

baseflow (Walvoord & Striegl 2007; St Jacques & Sauchyn 2009; Brabets & Walvoord 2009; Lyon & Destouni 2010). During winter, Alaskan ice-covered rivers are fed entirely by GW. Therefore, increased winter baseflow is likely due to increased GW input as a consequence of permafrost degradation associated with the increased GW input corresponding with permafrost degradation (Walvoord & Striegl 2007; St Jacques & Sauchyn 2009, Brabets & Walvoord 2009, Lyon & Destouni 2010) in discontinuous permafrost regions.

Heat from GW upwelling can degrade river ice from below. Field observations show that GW heat flux exceeds atmospheric heat losses and that dangerously thin ice conditions can be maintained for extended periods despite very cold wintertime air temperatures (Figure 1). In recent decades, there have been several reports that thin ice and open water may be more prevalent on interior Alaskan rivers in winter (Herman-Mercer *et al.* 2011; Jones *et al.* 2013; Schneider *et al.* 2013b), which are consistent with independent data on changes in regional hydrology. These conditions appear to be caused by a combination of factors that include fast-moving turbulent water, warmer air temperatures, and GW upwelling in shallow areas.

The Tanana Flats, which are found to the south of the Tanana River, have a high GW table and have exhibited extensive permafrost degradation since the 1700s (Jorgenson *et al.* 2001). Much of the Tanana River and its neighboring regions appear to be fed by GW upwelling. The observations of increased thin ice and open water on the Tanana during winter are hypothesized to be caused by increased GW flow caused by permafrost degradation, which has been intensified by a warming climate.

In this paper, fluctuations in GW hydrology were modeled to assess the potential impacts on river ice dynamics. In collaboration with rural Alaskans, changes in hydrology were explored to examine how residents of interior Alaska could be affected by recurring dangerous ice conditions in the Tanana River. Field studies were initiated in locations identified by local residents as having recurring thin ice. Based upon field observations, a numerical model was developed to explore the relationship between seasonal GW flow and ice thickness under changing environmental

Figure 1 | The Hot Cake Slough study site maintains open water during extended cold periods (−30 °C in this image).

conditions. The model was designed to address two primary research questions:

1. What physical factors have the greatest influence on seasonal dynamics between river ice thickness and GW upwelling on the Tanana River?
2. How do variations in environmental conditions change the capacity of GW to melt river ice?

METHODS

Field studies

Study sites were established in areas known to have dangerously thin ice. For modeling, we use data from Hot Cake Slough which is located within the Bonanza Creek Long-Term Ecological Research (LTER) area on the Tanana River, approximately 15 km southwest of Fairbanks, Alaska, USA (longitude: 148° 7′ 22″; latitude: 64° 43′ 26″) (Figure 2). This region is characterized by discontinuous permafrost and is bordered by the Tanana Flats region, which is part of the Tanana–Kuskokwim Lowlands (Anderson 1970). The Tanana Flats is an area with a high water table fed by GW originating from glaciers in the Alaska Range found to the south. The Alaska Range glaciers (typically found above 1,525 m) are considered as the primary source of water for the Tanana River (120 m elevation at Hot Cake Slough) (Anderson 1970).

Hot Cake Slough has a persistent open water feature that typically remains ice-free during much of the winter, but often attains a thin ice cover during extended cold (−25 to −40 °C) periods. A time-lapse camera taking daily photographs of the study area clearly showed the dynamic nature of the ice conditions. The water depth (measured

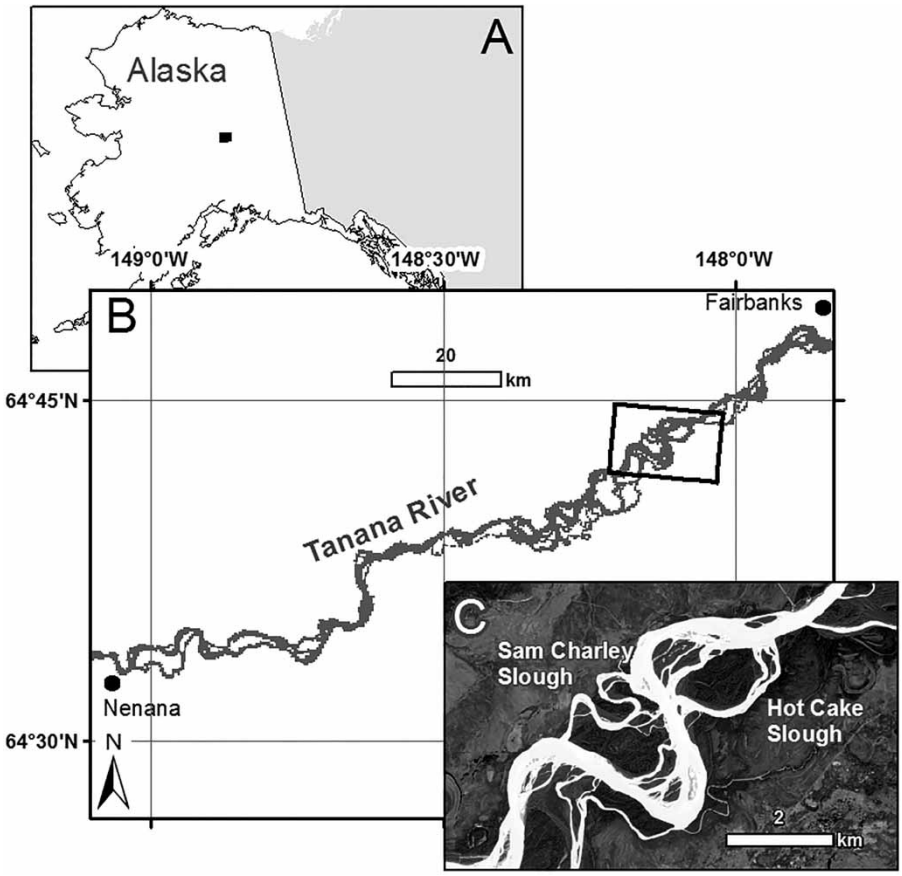

Figure 2 | Study area map of Hot Cake Slough of the Tanana River in Alaska. Panel A illustrates the position of Panel B within the state of Alaska. Panel B shows the position of Panel C relative to Fairbanks. Panel C shows the slough locations.

from channel floor to the bottom of the ice), channel velocity, and ice-free winter discharge were measured using a wading rod and a Marsh McBirney Flow-mate 2000 electromagnetic flow meter. Channel slope was measured using a level over a distance of 100 m. The local hydraulic conductivity (K, m/day) of the sediment within the open water feature of Hot Cake Slough was measured at a streambed sediment depth of 20 cm using the falling head permeameter method (Todd & Mays 2005). Nested piezometers (installed from 20 to 120 cm below channel thalweg) were installed in the open water feature of Hot Cake Slough and were used to measure the hydraulic gradient (dh/dz, dimensionless). From the measured hydraulic conductivity and hydraulic gradient, the vertical GW flow velocity (Q_{GWz}, m/day) was calculated using Darcy's Law (Todd & Mays 2005).

Salinity tracers were used to measure the horizontal GW flow velocity (V_{GWx}, m/day) between shallow (1.6 m) GW wells (Todd & Mays 2005). Using horizontal and vertical flow velocities, the total GW flow (Q_{GW}, m^3/d) into the channel at Hot Cake Slough was calculated per unit area (m^2).

The vertical temperature profile from the GW through the water column, ice, snow, and air within the river channel was measured at two different points in Hot Cake Slough (referenced as the upstream and downstream study sites). The temperature profile was monitored using thermistor strings calibrated to 0.0 °C in a continuously flowing ice bath.

Groundwater effect on water column temperature

The physical system is represented by Figure 3, which illustrates how GW affects river ice thickness under observed field conditions. From Figure 3, a physically based numerical model was developed using MATLAB® (version 2011b) to explore the heat balance between GW discharge and thermally degraded ice-covered areas. The model estimates the potential ice melt rate associated with GW under uniform and steady-state conditions (wind velocity, snow density, upwelling rate, GW temperature, air temperature, and snow depth). Ice-free circumstances are not considered in this model. Symbol definitions and units are summarized in the Appendix (available online at http://www.iwaponline.com/nh/046/026.pdf).

The heat flux (Equation (1)) for a system with lateral water flow into and out of a volumetric cell was modeled

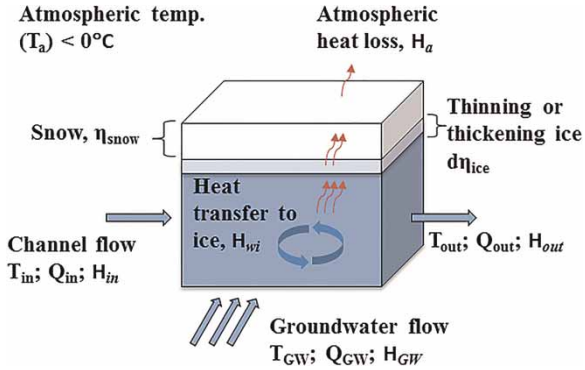

Figure 3 | A conceptual diagram of how heat transfer from GW affects river ice conditions in sub-arctic rivers (see variable definitions in the Appendix, available online at http://www.iwaponline.com/nh/046/026.pdf).

with vertical GW flow. Each flow stream was associated with an energy flux [H ($W \cdot m^{-2}$)] (Figure 3). Energy was transferred from the water column to the ice (H_{wi}). The water column warmed when the GW heat energy flowing into the water column ($H_{in} + H_{GW}$) was greater than H_{wi}, or cooled when H_{wi} was greater than $H_{in} + H_{GW}$. Assuming the presence of freezing air temperatures, the heat transferred to the ice was either lost to the atmosphere (H_a) or melted ice (H_m) (Equation (2)).

$$0 = H_{in} + H_{GW} - H_{wi} - H_{out} \quad (1)$$

$$H_{wi} = H_a + H_m \quad (2)$$

The surface and GW flow had a specified flow rate (Q, $m^3 \cdot s^{-1}$) and average temperature (T, °C) from which the heat flux of each component was calculated (Equation (3)) relative to the melting temperature of ice (T_m, 0 °C) using water's volumetric heat capacity (C_v, $J \cdot m^{-3} \cdot °C^{-1}$). The model assumed thorough mixing of ground and surface water.

$$H = C_v Q\,(T - T_m) \quad (3)$$

The heat transfer rate from the water to the ice was calculated for turbulent flow using established empirical relationships (Equation (4)) between the Nusselt number ($Nu = H_w \cdot R(T - T_m)^{-1} k^{-1}$), the Reynolds number ($Re = U_w R \rho \mu^{-1}$), and Prandtl number ($Pr = \mu C_p\ k^{-1}$) (Ashton 1982). In these equations, the corresponding symbols

represent the heat flux of water (H_w), hydraulic radius (R, m), thermal conductivity of water (k, $W{\cdot}m^{-1}{\cdot}K^{-1}$), water velocity ($U_w$, $m{\cdot}s^{-1}$), water density (ρ, kg/m^3), and dynamic viscosity (μ, $kg{\cdot}m^{-1}{\cdot}s^{-1}$). The coefficient C is approximately 0.023 (which may be up to 50% greater for ice that is not smooth on its underside) (Ashton 1982).

$$u = C\mathrm{Re}^{0.8}\mathrm{Pr}^{0.4} \tag{4}$$

A heat transfer coefficient (h_{wi}, $W{\cdot}m^{-2}{\cdot}^{\circ}C$) was used to model the heat transfer rate between water and ice (Ashton 1982). In previous studies, it has been calculated empirically or analytically and applied to Equation (3) in the form of Equation (5) (Williams 1963; Ashton 1982, 2010; Wankiewicz 1984; Calkins 1984; Marsh & Prowse 1987).

$$H_{wi} = h_{wi}(T - T_m) \tag{5}$$

Equation (4) was rewritten for the heat transfer coefficient in the form, $h = (Ck/R)\mathrm{Re}^{0.8}\mathrm{Pr}^{0.4}$ and was transformed into Equation (6) by substituting numerical values for the properties of water, using $C = 0.023$, replacing R with $D/2$, and using SI units (Ashton 1982).

$$h_{wi} = 1622U_w^{0.8}D^{-0.2} \tag{6}$$

Equations (5) and (6) were applied to calculate H_{wi}, which was used with H_{in} and H_{GW} (Equation (3)) to calculate H_{out} (Equation (1)) and estimate T_{out} from Equation (3). T_{out} could be utilized to model changes in heat flux in the downstream direction.

Atmospheric heat losses and ice melt

As depicted by Equation (2), assuming freezing air temperatures (T_a, $^{\circ}C$), the heat transferred from the water to the ice was either lost to the atmosphere via conduction or contributed to ice melt. The temperature at the bottom of the ice was assumed constant ($T_m = 0\,^{\circ}C$), but the thickness (η, m) and thermal conductivity (k, $W{\cdot}m^{-1}{\cdot}^{\circ}C^{-1}$) of the ice and snow, combined with atmospheric conditions affected the heat lost to the atmosphere (Equation (7)) (Ashton 1982, 2010). k_{snow} was estimated from snow density (Sturm *et al.* 1997) and the surface resistance of the boundary layer (m, $m^2{\cdot}^{\circ}C{\cdot}W^{-1}$) was approximated using the wind velocity (U_a, $m{\cdot}s^{-1}$) in $(10 + U_a)^{-1}$ (Starosolszky 1968).

$$H_a = \frac{T_m - T_a}{\frac{\eta_{ice}}{k_{ice}} + \frac{\eta_{snow}}{k_{snow}} + m} \tag{7}$$

By combining Equations (2)–(7), the rate of ice thickness change ($\Delta\eta_{ice}/\Delta t$, $m{\cdot}day^{-1}$) was approximated from the latent heat of fusion for water (F, $J{\cdot}kg^{-1}$) and the density of ice (ρ_{ice}, $kg{\cdot}m^{-3}$) (Equation (8)) (Ashton 1982, 2010). The potential ice melt rate equals $-\Delta\eta_{ice}/\Delta t$.

$$\frac{\Delta\eta_{ice}}{\Delta t} = \frac{1}{F\,\rho_{ice}}\left[\frac{T_m - T_a}{\frac{\eta_{ice}}{k_{ice}} + \frac{\eta_{snow}}{k_{snow}} + m} - 1622U_w^{0.8}D^{-0.2}(T_w - T_m)\right] \tag{8}$$

Unsteady flow conditions

Unsteady flow was modeled similarly by examining how continuous GW inputs would affect ice thickness in a downstream direction in a channel under field conditions. Simulating movement in a downstream direction, water depth of the volumetric cell was estimated, assuming subcritical flow based upon the incoming water depth and the volumetric flow of GW into the cell. Flow velocity was calculated using Manning's Equation for SI units ($U_w = R^{2/3}S^{1/2}n^{-1}$, $m{\cdot}s^{-1}$) (Sturm 2001) using the hydraulic radius (R), the calculated water surface slope (S), and an estimated composite Manning's coefficient ($n = 0.03$, dimensionless), which accounts for ice cover and channel roughness.

The initial air temperature, ice thickness, snow depth, and wind velocity were specified. Freezing air temperatures and snow depth could change over time, but wind velocity was assumed constant. The heat transfer coefficient was calculated from the average measured water column temperature ($T_w = 1.4\,^{\circ}C$), while GW temperature was assumed $3.2\,^{\circ}C$ based on field measurements.

Thermal equilibrium

To examine the steady-state model at equilibrium conditions, theoretical scenarios were used to examine the

system when the total energy gained from GW equaled the energy transferred to the ice, which equaled the energy lost to the atmosphere ($H_{GW} = H_{wi} = H_a$). In the first assessment, H_{GW} input was based upon field measurements ($T_{GW} = 3.2\ ^{\circ}C$ and $Q_{GW} = 0.85\ m{\cdot}day^{-1}$). H_{wi} was adjusted by modifying T_w until H_{wi} was equal to H_{GW}. H_a was adjusted by modifying T_a until H_a was equal to H_{GW}. In the second assessment, T_a was assumed ($-23\ ^{\circ}C$) based upon field observations when open water was just beginning to freeze ($\Delta\eta_{ice} = 0.001$ m) and H_a was calculated. H_{wi} was adjusted by modifying T_w until H_{wi} was equal to H_a. H_{GW} was adjusted by modifying Q_{GW} until H_{GW} was equal to H_a. In a third assessment, the GW and surface water temperatures were assumed ($T_w = 1.4\ ^{\circ}C$ and $T_{GW} = 3.2\ ^{\circ}C$), while T_a and U_{GW} were adjusted until $H_{GW} = H_{wi} = H_a$.

Sensitivity analyses

Analyses were performed to estimate the sensitivity of the model to changes in the dominant input variables. Specific initial conditions were used as model input for the standard analyses (Table 1). Each input variable was increased and decreased by 30% to determine the resulting sensitivity of the ice melt calculation. The 30% change in each input variable was selected as a reasonable, yet consistent proportional modification to assess the relative response of the model.

Confidence analysis

A confidence analysis was performed to estimate model performance relative to the estimated measurement accuracy of each input variable (Table 2). Modified input

Table 1 | Sensitivity analysis assessing the model's response to changes in input variables at the specified initial conditions

Variable	Units	Initial	Variability	Sensitivity of ice melt rate
$T_w - T_m$	$^{\circ}C$	1.4	± 30%	± 68%
Water velocity	$m{\cdot}s^{-1}$	0.02	± 30%	−53 to +56%
$T_a - T_m$	$^{\circ}C$	−10	± 30%	± 38%
Water depth	Cm	20	± 30%	−12 to +17%
Snow depth	Cm	10	± 30%	−13 to +11%
Wind speed	$m{\cdot}s^{-1}$	0.5	± 30%	± 2%
$T_{GW} - T_m$	$^{\circ}C$	3.2	± 30%	± 0%
GW upwelling rate	$m{\cdot}day^{-1}$	0.86	± 30%	± 0%
Initial ice thickness	Cm	10	± 30%	± 0%

Table 2 | Model confidence analysis assessing the effect of potential measurement errors

Variable	Units	Initial	Measurement confidence	Total estimated confidence in modeled ice melt rate
$T_w - T_m$	$^{\circ}C$	1.4	± 0.5%	Melt estimate = 18 mm/day (confidence range ± 16%)
Water velocity	$m{\cdot}s^{-1}$	0.02	± 0%	
$T_a - T_m$	$^{\circ}C$	−10	± 0.5%	
Water depth	Cm	20	± 0.5%	
Snow depth	Cm	10	± 0.5%	
Wind speed	$m{\cdot}s^{-1}$	0.5	± 50%	
$T_{GW} - T_m$	$^{\circ}C$	3.2	± 0.5%	
GW upwelling rate	$m{\cdot}day^{-1}$	0.86	± 30%	
Initial ice thickness	Cm	10	± 1.0%	

values were varied by increasing and decreasing the initial value by its estimated accuracy (%). All of the modified input values that would maximize (or minimize) the ice melt rate were used simultaneously to determine how uncertainty of the input variables affected model output.

RESULTS

Field studies

The water depth showed little variation from December through early April each year (varying less than 1 cm until mid-April). The average water velocity of the upstream channel cross-section was 0.02 $m \cdot s^{-1}$. The channel slope was measured to be less than 0.001 and when calculated from the Manning's Equation for the observed conditions (with Manning's $n = 0.03$), the slope was calculated to be less than 0.00001. The vertical hydraulic conductivity (K) was measured to be 4.0 $m \cdot day^{-1}$. The vertical hydraulic gradient varied with the depth of each piezometer. The 1.90 m deep piezometer had a consistently lower flow rate than the 1.10 m deep piezometer. For April 2013, the average piezometric head at 1.10 m depth was 0.085 m (s.d. = 0.022) across a vertical distance of 0.44 m (Figure 4) and the calculated vertical GW flow rate averaged 0.77 $m \cdot day^{-1}$ (s.d. = 0.20) (Figure 4). One outlier of piezometric head was omitted from the analysis. On two different days, horizontal GW velocities were measured to be 0.5 and 0.3 $m \cdot day^{-1}$ at a depth of 1.6 m, which corroborates measurements of 0.3 $m \cdot day^{-1}$ reported by Clilverd *et al.* (2008) in similar substrates from nearby LTER sites. With these GW flow rates and a channel depth of 20 cm, the total average GW velocity into the channel was calculated to be 0.86 $m \cdot day^{-1}$.

In March 2013, the vertical temperature profile measured nearly constant GW temperatures of 2.7 °C at a depth 0.5 m below the thalweg at the upstream site in Hot Cake Slough (Figure 5), while the downstream site in Hot Cake Slough had a GW temperature of 3.2 °C (Figure 6). At the upstream site, the water column temperature averaged 1.4 °C (Figure 7(a)), while the downstream site water column averaged 1.7 °C (Figure 7(b)).

Time-lapse photos were used to observe site conditions on a daily basis (Figure 1). Using the photo series, changes in site conditions were observed over three different winter seasons. Notably, despite much colder air temperatures in the winter 2011–2012, there was more open water in Hot Cake Slough than in the winter of 2012–2013. Data were insufficient from the 2010–2011 season to compare the period of ice cover to 2012–2013.

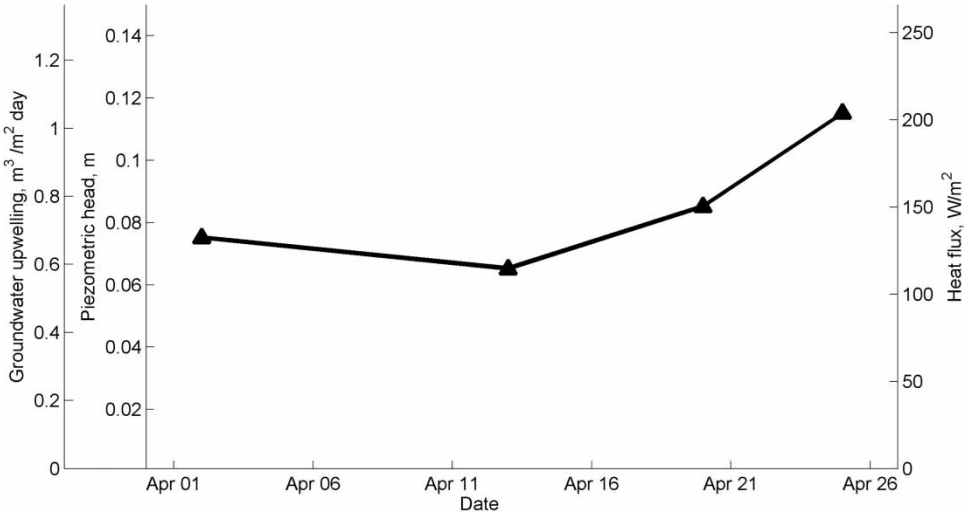

Figure 4 | The piezometric head that measured 1.10 m beneath the thalweg of Hot Cake Slough was used to calculate the vertical GW upwelling rate and the vertical GW heat flux for spring 2013. All three *y*-axes are represented by the same line on the figure.

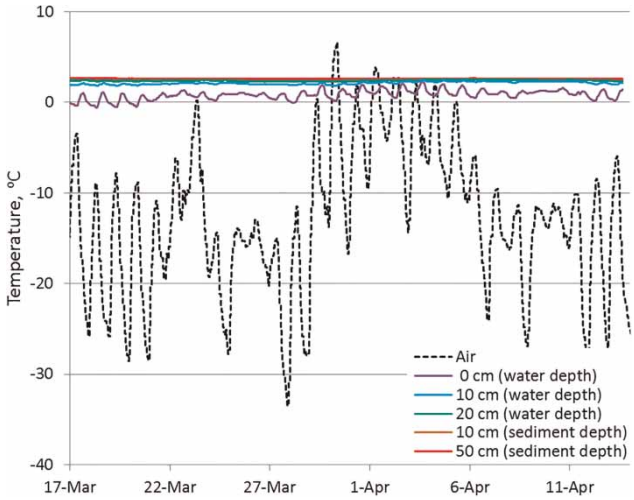

Figure 5 | Vertical temperature profile at the upstream field site in Hot Cake Slough. This figure illustrates how water temperature near or beneath the channel bottom is nearly constant, while temperatures near the water surface oscillate with air temperature (data from 2013).

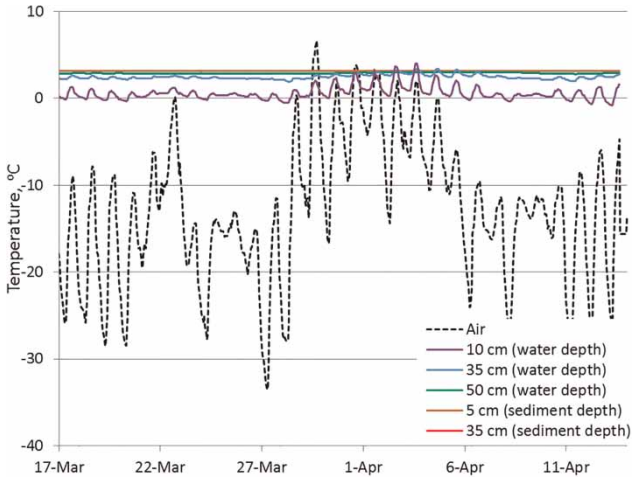

Figure 6 | Vertical temperature profile at the downstream field site in Hot Cake Slough. This figure illustrates how the GW temperatures near or beneath the channel bottom are nearly constant, while water temperatures near the water surface oscillate relative to changes in air temperature (data from 2013).

Modeling

According to Equation (8), the potential ice melt rises with increasing air temperature, water column temperature, initial ice thickness, initial snow depth, or water velocity, but falls with rising water depths. The water column temperature increases with increased GW upwelling rates and GW temperatures, both of which increase the GW heat

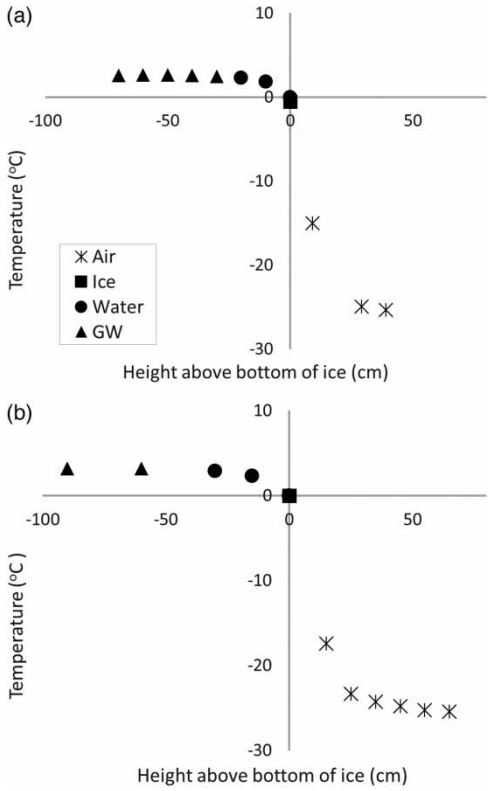

Figure 7 | Vertical temperature profiles from 8 a.m. on 18 March 2013 at the upstream (a) and downstream (b) monitoring stations in the Hot Cake Slough of the Tanana River in Alaska.

flux (Equation (3)). At a GW upwelling temperature of 3.2 °C, the measured GW heat flux (133 $W \cdot m^{-2}$) would melt up to 3.8 cm of ice per day under ideal conditions with no heat lost to the atmosphere or gained by the water column.

Snow-free ice that was 10 cm thick was modeled to melt at the measured GW upwelling rate (0.86 $m \cdot day^{-1}$) when the average water temperature was 1.4 °C and air temperatures were −14 °C or greater (Figure 8(a)). However, the presence of snow radically changes these relationships (Figure 8(b)). At the temperatures down to −40 °C (while including conductive and convective heat losses), the ice would melt with only 5 cm of snow. Moreover, the variability in ice melt rates associated with colder air temperatures is tempered by increasing snow cover (Figure 8(b)) and ice melt is largely independent of air temperatures when snow depths are greater than 10 cm (measured snow density = 395 $kg \cdot m^{-3}$). This depth represents the 'hiemal threshold' (Pruitt Jr 1957), which

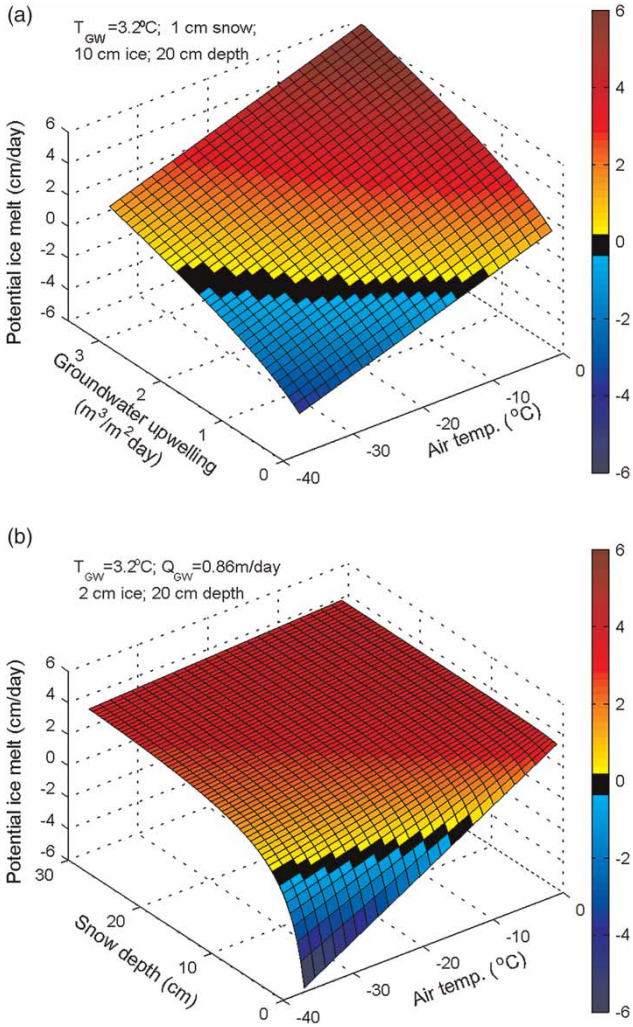

Figure 8 | Melt rate response curves over a range of air temperatures and GW upwelling rates (a) or snow depths (b) given specific initial conditions (noted in the upper left). Color bar on the right represents the potential ice melt (cm day^{-1}).

varies according to snow density, but is defined as the snow depth at which the physical and biological systems under the snow are thermally isolated from oscillations in air temperature.

At a snow depth of 1 cm, the air temperature is directly proportional to the potential ice melt, while increasing GW flow results in a non-linear increase in the ice melt rate (Figure 8(a)). Similarly, the complexity of the response surface of the potential ice melt rate over a range of snow depths and air temperatures (Figure 8(b)) show that the importance of air temperature is attenuated with increasing snow depth. It also illustrates the linear response of ice melt relative to changes in air temperature and the steep response gradient at low snow depths.

Thermal equilibrium

In the assessment where GW measurements were assumed accurate ($U_{GW} = 0.86$ m·day^{-1}; $T_{GW} = 3.2$ °C) in a system at thermal equilibrium, $H_{GW} = 133$ W·m^{-2}. To be in equilibrium under these conditions ($\eta_{ice} = 2$ cm and $\eta_{snow} =$ 1 cm), T_w would be 1.4 °C at T_a of −19 °C. In an assessment assuming water column temperatures were accurate (mean $T_w = 1.4$ °C, mean $T_{GW} = 3.2$ °C, $\eta_{ice} = 0.2$ cm; $\eta_{snow} =$ 1 cm), $H_{ice} = 136$ W·m^{-2}. T_a would be −19 °C and U_{GW} would be 0.87 m·day^{-1} at thermal equilibrium. In the assessment where field observations of T_a were used while water was starting to freeze ($T_a = -23.0$ °C; $\eta_{ice} = 0.1$ cm; $\eta_{snow} =$ 0 cm), $H_a = 230$ W·m^{-2}. At thermal equilibrium under these conditions, U_{GW} would be 1.48 m·day^{-1} with $T_{GW} =$ 3.2 °C and T_w would be 2.4 °C.

Sensitivity analysis

Table 1 shows that the calculated ice melt rate was most sensitive to increases in the water column temperature, water velocity, air temperature, water depth, and snow depth, respectively. The sensitivity of each variable is dependent on the initial conditions. At the conditions specified (Table 1), a 30% change in the water temperature, water velocity, air temperature, water depth, or snow depth would affect the ice melt calculations by more than 10% (Table 1).

Confidence analysis

A confidence analysis was performed to gain an understanding of model performance based upon the measurement confidence of the input variables. Under the assumption that each input variable has errors associated with its measurement, confidence in model performance would decrease with increasing measurement errors. Table 2 suggests that if the estimated minimum and maximum errors of all input variables were realized simultaneously, the modeled ice melt rate

could range from ±16% of the initial output value of 18 mm·day^{-1} (e.g., 15–20 mm·day^{-1}).

DISCUSSION

Degrading permafrost, warming air temperatures, forest fires, or changes in precipitation are factors that could affect GW flow rates. Walvoord & Striegel (2007) hypothesized that permafrost degradation has caused the 20% increase in observed winter GW discharge in the Tanana River between 1963 and 2005. Increased air temperatures associated with climate have increased permafrost temperatures and can transform discontinuous permafrost zones into areas without permafrost (Rowland *et al.* 2010; Romanovsky *et al.* 2010). These factors increase water exchange rates between surface and ground water (Hinzman *et al.* 2013) and in areas with a positive hydraulic gradient (GW pressure), upwelling rates will increase.

Field observations suggested that GW upwelling decreased river ice thickness under winter conditions in interior Alaska (Jones *et al.* 2013; Jones 2014). Increased snow accumulation would increase the thermal insulation of the ice, decrease the heat losses from the water column to the air, and leave more heat energy available for degrading ice. While GW flow into the channel maintained a 2.7 to 3.2 °C temperature gradient between the channel bottom and the bottom of the ice, the thermal gradient between the water column and the air temperature was tempered by the constant temperature at the bottom of the ice. Modeling results suggest that GW temperatures played a minor role in melting the ice relative to other parameters (Table 1), contrary to field observations. Water column temperature and flow velocity were modeled to be the most important drivers of ice degradation. Water column temperature and velocity are both affected by GW input, but the GW measurements suggest that only 0.25% of channel flow is attributable to GW for each meter of the flow path. The cumulative downstream effect of GW flow on an ice-covered channel was not modeled, but could be a future extension of the research.

Groundwater velocities are inherently difficult to measure during winter field conditions. The modeling results suggest that GW flows were not measured with sufficient spatial or temporal resolution to capture their variability. Whereas GW flow was measured, preferential GW flow paths may exist that were not sampled during field measurements. The locations of maximum vertical GW flux were sought, but could only be identified by the presence of open water. In addition, hydraulic conductivity was measured at a shallower depth than the maximum vertical flux was measured. Therefore, it is probable that the hydraulic conductivity of preferential flow paths was higher than measured and winter GW flow rates were higher than calculated. If the flow rate was higher, the GW and surface water may have mixed less and GW temperatures may have been higher than measured, which would increase the GW heat flux (Kurylyk *et al.* 2013, 2014) and the ice melt rate (Jones *et al.* 2013).

Of the dominant environmental factors (Table 1), air temperature and snow depth change most rapidly. Modeling results suggest that changes in the timing or magnitude of snow accumulation influenced the potential ice melt rates affiliated with GW. The effect of air temperature on ice melt rate was attenuated as snow accumulated on the ice (Figure 8(b)). During late winter in interior Alaska, snow depths typically exceed the hiemal threshold, thereby thermally isolating the water column from air temperature oscillations. Assuming stable channel morphology, water velocity and depth were not expected to vary significantly through the winter months after stabilizing in November or December, although the proportion of GW to surface water would increase slowly through the winter.

CONCLUSIONS

Rural Alaskans have observed that winter travel conditions have become more dangerous due to thin or open ice in recent memory (Herman-Mercer *et al.* 2011; Schneider *et al.* 2013a, b). Researchers observed slow-moving open water at temperatures as low as −30 °C (Figure 1), but modeling results suggest that field measurements of GW flow (hydraulic conductivity, vertical gradient, and horizontal velocity) were not sufficient to maintain open water conditions. This research suggests that more extensive characterization of GW flow paths would be necessary to model the influence of GW even in areas of limited spatial

extent. It was hypothesized that degrading permafrost in distant recharge areas could allow for enhanced infiltration and greater fluxes in GW upwelling areas to melt ice from below to generate hazardous ice conditions; however, the results of this study were inconclusive and suggest that additional study would be warranted.

In sub-arctic environments, winter travel on rivers is common, especially in the context of subsistence activities. Predictable and reliable environmental conditions help maintain the quality of life for subsistence peoples. While subsistence peoples are adaptable, environmental variability increases their vulnerability to cultural disruptions that include individual or household decisions to migrate from subsistence lifestyles in remote communities to jobs in cash-based economies in cities. This study illustrates the importance of using applied science to investigate the complex interactions between climate, hydrology, and society to understand how increasing variability in climate and natural processes may affect the lives of subsistence users in the north.

ACKNOWLEDGEMENTS

This research was made possible by the generous partnership with the Village of Tanana, Alaska and the individuals that assisted with this research. We especially would like to express our gratitude for the support and efforts of our collaborators, including Ruth Althoff, Karen Brewster, Charlie Campbell, Wallie Carlo, Sam Dementieff, Ronnie Evans, Kristy Johnson, Dave Norton, Karl Olsen, Neil Scannell, Marla Statscewich, Matthew Sturm, and Charlie Wright. This research was supported by the National Science Foundation's (NSF) Division of Polar Programs (grants OPP-0422068, ARC-0517762, and ARRA ARC-0909517), NSF's 'Resilience and Adaptation of Social-Ecological Systems in a Rapidly Changing North' IGERT program (grant #0654441), and the Bonanza Creek Long-Term Ecological Research program (DEB-10226415). Additional support was provided by the International Arctic Research Center, Alaska EPSCoR NSF (OIA-1208927) with the state of Alaska, Alaska Climate Science Center, UAF Water and Environmental Research Center, UAF Center for Global Change Student Research Grant, and the USGS through the National Institutes for Water Research program. The views expressed in the paper are those of the authors and do not represent the funding agencies.

REFERENCES

Anderson, G. S. 1970 Hydrologic reconnaissance of the Tanana Basin, central Alaska: U.S. Geological Survey Hydrologic Investigations Atlas (HA-319). Washington, DC (available online at: www.dggs.alaska.gov/pubs/id/13643).

Ashton, G. D. 1982 Theory of thermal control and prevention of ice in rivers and lakes. In: *Advances in Hydroscience* (V. T. Chow, ed.). Academic Press, New York, USA, pp. 132–183.

Ashton, G. D. 2010 *River Lake Ice Engineering* (G. D. Ashton, ed.), 3rd edn. Water Resources Publications, LLC, Highlands Ranch, CO, USA, 485 pp.

Brabets, T. P. & Walvoord, M. A. 2009 Trends in streamflow in the Yukon River Basin from 1944 to 2005 and the influence of the Pacific Decadal Oscillation. *J. Hydrol.* **371**, 108–119.

Burt, T. P. & Williams, P. J. 1976 Hydraulic conductivity in frozen soils. *Earth Surf. Process.* **1**, 349–360.

Calkins, D. J. 1984 Ice cover melting in a shallow river. *Can. J. Civ. Eng.* **11**, 255–265.

Clilverd, H. M., Jones, J. B. & Kielland, K. 2008 Nitrogen retention in the hyporheic zone of a glacial river in interior Alaska. *Biol. Chem.* **88**, 31–46.

Herman-Mercer, N., Schuster, P. F. & Maracle, K. B. 2011 Indigenous observations of climate change in the lower Yukon River basin, Alaska. *Hum. Organ.* **70**, 244–252.

Hinzman, L. D., Bettez, N. D., Bolton, W. R., Chapin III, F. S., Dyurgerov, M. B., Fastie, C. L., Griffith, B., Hollister, R. D., Hope, A., Huntington, H. P., Jensen, A. M., Jia, G. J., Jorgenson, M. T., Kane, D. L., Klein, D. R., Kofinas, G. P., Lynch, A. H., Lloyd, A. H., McGuire, A. D., Nelson, F. E., Oechel, W. C., Osterkamp, T. E., Racine, C. H., Romanovsky, V. E., Stone, R. S., Stow, D. A., Sturm, M., Tweedie, C. E., Vourlitis, G. L., Walker, M. D., Walker, D. A., Webber, P. J., Welker, J. M., Winker, K. S. & Yoshikawa, K. 2005 Evidence and implications of recent climate change in northern Alaska and other arctic regions. *Clim. Change* **72**, 251–298.

Hinzman, L. D., Deal, C. J., McGuire, A. D., Mernild, S. H., Polyakov, I. V. & Walsh, J. E. 2013 Trajectory of the Arctic as an integrated system. *Ecol. Appl.* **23**, 1837–1868.

Horiguchi, K. & Miller, R. D. 1980 Experimental studies with frozen soil in an 'ice sandwich' permeameter. *Cold Reg. Sci. Technol.* **3**, 177–183.

Jones, C. E. 2014 *The Integrated Hydrologic and Societal Impacts of a Warming Climate in Interior Alaska*. PhD Thesis. Institute of Northern Engineering, University of Alaska Fairbanks, Fairbanks, Alaska.

Jones, C. E., Kielland, K. & Hinzman, L. D. 2013 Modeling groundwater upwelling as a control on river ice thickness. In:

Proceedings of the 19th International Northern Research Basins Symposium and Workshop (S. L. Steufer & W. R. Bolton, eds). University of Alaska Fairbanks, Fairbanks, Alaska, USA. August 11–17, 2013, pp. 107–115.

Jorgenson, M. T., Racine, C. H., Walters, J. C. & Osterkamp, T. E. 2001 Permafrost degradation and ecological changes associated with a warming climate in central Alaska. *Clim. Change* **48**, 551–579.

Kane, D. L. & Stein, J. 1983 Water movement into seasonally frozen soils. *Water Resour. Res.* **19**, 1547–1557.

Kurylyk, B. L., Bourque, C. P. A. & MacQuarrie, K. T. B. 2013 Potential surface temperature and shallow groundwater temperature response to climate change: an example from a small forested catchment in east-central New Brunswick (Canada). *Hydrol. Earth Syst. Sci.* **17**, 2701–2716.

Kurylyk, B. L., MacQuarrie, K. T. B. & Voss, C. I. 2014 Climate change impacts on the temperature and magnitude of groundwater discharge from shallow, unconfined aquifers. *Water Resour. Res.* **50**, 3253–3274.

Lyon, S. W. & Destouni, G. 2010 Changes in catchment-scale recession flow properties in response to permafrost thawing in the Yukon River basin. *Int. J. Climatol.* **30**, 2138–2145.

Marsh, P. & Prowse, T. D. 1987 Water temperature and heat flux at the base of river ice covers. *Cold Reg. Sci. Technol.* **14**, 33–50.

Pruitt Jr, W. O. 1957 Observations on the bioclimate of some taiga mammals. *Arctic* **10**, 129–138.

Romanovsky, V. E., Smith, S. L. & Christiansen, H. H. 2010 Permafrost thermal state in the polar northern hemisphere during the international polar year 2007–2009: a synthesis. *Permafr. Periglac. Process.* **21**, 106–116.

Rowland, J. C., Jones, C. E., Altmann, G., Bryan, R., Crosby, B. T., Hinzman, L. D., Kane, D. L., Lawrence, D. M., Mancino, A., Marsh, P., McNamara, J. P., Romanovsky, V. E., Toniolo, H., Travis, B. J., Trochim, E., Wilson, C. J. & Geernaert, G. L. 2010 Arctic landscapes in transition: responses to thawing permafrost. *Eos* **91**, 229–230.

Schneider, W., Brewster, K., Kielland, K. & Jones, C. E. 2013a *On dangerous ice: Changing ice conditions on the Tanana River*. University of Alaska Fairbanks, Fairbanks, Alaska. 76 pp.

Schneider, W., Stephens, S., McCartney, L., Brewster, K. & Statscewich, M. 2013b Alaska stakeholders & climate change. http://jukebox.uaf.edu/site/stakeholders.

Smith, L. C., Sheng, Y. & MacDonald, G. M. 2007 A first pan-Arctic assessment of the influence of glaciation, permafrost, topography and peatlands on northern hemisphere lake distribution. *Permafr. Periglac. Process.* **208**, 201–208.

Starosolszky, O. 1968 *Ice in Hydraulic Engineering*. Division of Hydraulic Engineering, Norwegian Institute of Technology, University of Trondheim, Norway. 165 pp.

St Jacques, J.-M. & Sauchyn, D. J. 2009 Increasing winter baseflow and mean annual streamflow from possible permafrost thawing in the Northwest Territories, Canada. *Geophys. Res. Lett.* **36**, 1–6.

Sturm, T. W. 2001 Chapter 4. Uniform flow. In: *Open Channel Hydraulics*, 3rd edn. McGraw-Hill Book Co., Singapore, pp. 97–157.

Sturm, M., Holmgren, J., Konig, M. & Morris, K. 1997 The thermal conductivity of seasonal snow. *J. Glaciol.* **43**, 26–41.

Todd, D. K. & Mays, L. W. 2005 Chapter 3: Groundwater movement. In: *Groundwater Hydrology*, 3rd edn. John Wiley & Sons, Hoboken, NJ, USA, pp. 86–145.

Walvoord, M. A. & Striegl, R. G. 2007 Increased groundwater to stream discharge from permafrost thawing in the Yukon River basin: potential impacts on lateral export of carbon and nitrogen. *Geophys. Res. Lett.* **34**, 1–6.

Wankiewicz, A. 1984 Analysis of winter heat flow in an ice-covered Arctic stream. *Can. J. Civ. Eng.* **11**, 430–443.

Williams, G. P. 1963 Heat transfer coefficients for natural water surfaces. *Int. Assoc. Sci. Hydrol.* **62**, 203–212.

Yoshikawa, K. & Hinzman, L. D. 2003 Shrinking thermokarst ponds and groundwater dynamics in discontinuous permafrost near Council, Alaska. *Permafr. Periglac. Process.* **14**, 151–160.

First received 30 January 2014; accepted in revised form 22 December 2014. Available online 27 January 2015